

# Computational Study of the Effect of Fin Longitudinal Spacing and Reynolds Number on the Performance of Oblique Heat Sinks

<sup>1</sup>Muhamad Safi'i, <sup>2\*</sup>Nazaruddin Sinaga, <sup>3</sup>Syaiful, <sup>4</sup>Sukiman

<sup>1,2,3</sup>Department of Mechanical Engineering, Faculty of Engineering, Diponegoro University, Jalan Prof. Soedarto, Tembalang, Semarang 50275, Central Java, Indonesia

<sup>4</sup>STIMA IMMI, Jalan Raya Tanjung Barat, Jakarta Selatan, Indonesia

<sup>1</sup>E-mail: [muhammadsyafii17@students.undip.ac.id](mailto:muhammadsyafii17@students.undip.ac.id)

<sup>2\*</sup>Corresponding Author's E-mail: [nsinaga19.undip@gmail.com](mailto:nsinaga19.undip@gmail.com)

**Abstract - Various heat sinks have been widely researched to get a better performance design. This research aims to study the effect of fin longitudinal spacing and Reynolds number on heat sink performance at an oblique angle of 45 degrees. This study utilizes a finite-volume computational approach to determine the performance and details of the flow on the heat sinks. The calculations are conducted on fin spacing between 0.3 mm and 1.5 mm in the Reynolds number of 6,470 to 19,410. It was found that the fin longitudinal spacing significantly affects the performance of heat sinks for various Reynolds numbers, where the larger the spacing, the higher the Nusselt number. Based on this study, it can be concluded that it is necessary to determine the optimal fin longitudinal spacing in the design of the oblique heat sink.**

**Keywords:** Heat sink, oblique, convection.

## I. INTRODUCTION

With the rapid development of micro-electronic systems, cooling is one of the main concerns in electronic devices to improve the performance of electronic systems [1]. Thus, an effective and efficient cooling technique is needed to eliminate heat transfer loads, increase heat transfer heat, and minimize excessive pressure drops in a suitable electronic system such as a heat sink. Heat sinks help maintain device performance in all conditions and as an effective and innovative cooling technology for electronic and microelectronic systems [2-5]. Heat sinks are widely used to cool electronic devices such as computer CPUs and LED lights [6,7].

Fan less heat sinks are preferred because of their compact size, noiselessness, and high power requirements [8,9]. Under these circumstances, convection and radiation are the main ways to improve heat transfer in the heat sink because they can increase radiant heat transfer [10]. However, a heat sink with a fan can be used with the forced convection method for air cooling to reduce pressure and improve the cooling

performance of the heat sink for the better [11]. Conduction heat transfer can also be applied to reduce the interfacial temperature. It can significantly increase the thermal conductivity of the heat sink due to the stream wise increase of fully developed hydrodynamic flow [12].

Various studies have been carried out both experimentally and numerically on heat transfer in heat sinks to know the increase in performance, performance, efficiency, and reducing the interface temperature and excess pressure on the heat sink [13-16]. Various heat sink designs and configurations have fin shape variations such as ovals, airfoils, circles, W-fin shapes, straight rectangles, and triangles [17-21]. The modified oblique fin shape with an angle between 30-45° modified from the straight fin heat sink was investigated to improve the heat transfer performance, and it can be demonstrated by the presence of flow induction around the fin surface and continuously initializing the thermal and hydraulic boundary layer [22].

The rippling fin shape was investigated to know the heat sink's flow characteristics and thermal performance. From the variation of the configuration, the effect on the heat sink performance and the decrease in pressure and thermal resistance can be seen. It can be proven by decreasing the fin surface regularity to 18.35 K and can reduce the thermal resistance by 9,81% [23]. The shape of the fin in the form of a bent shape by 90° was investigated to increase the turbulence grid eddies to increase convective heat transfer in the heat sink with a very high percentage of 57-60% [24].

The shape of the groove on the ventral surface of the heat sink fin is characterized by varying the bubble volume and incoming heat flux to improve heat transfer in the heat sink. With the influence of various groove geometry shapes such as circles, rectangles, triangles, and rhombuses to the distance and thickness of the fins as well as the incoming heat power to increase the thermal conductivity of the heat sink,

theadvantageofthegrooveshape is toincreasetheflow area andreducepressure drop [25].

contours experimentally and numerically to increase the heat transfer coefficient in the heat sink [34]. Heat transfer for heat configuration sinks with various materials, such as aluminium, can increase the thermal conductivity and heat transfer of the heat sink fins [35]. Copper material is also used to characterize heat transfer in the heat sink [36]. Multi-phase flow (single-phase and two-phase) in heat sinks with micro-channels can also be used as a cooling fluid property because of the uniform temperature distribution in the fin surface area [37]. In research related to heat sinks, optimization can be used as a reference for designing the micro channel heat sinks using the COMSOL program on heat sinks with various variations such as length and height of fins to know the heat conduction structure of the heat sink [38, 39]. Besides, therewasalsoaninvestigationrelated to heat sinks with spiral heat sink fins with a nanofluid [40].

| Nomenclature |   | Subscript     |  |
|--------------|---|---------------|--|
| $A_b$        | Base area ( $m^2$ )                     | Ave           | Average  |
| C            | Weakly flow ( $N/m^2$ )                 | b             | Bottom   |
| $C_p$        | Specific heat ( $J/kg^{\circ}C$ )       | ba            | Base   |
| $D_h$        | Hydraulic diameter                      | Ch            | Channel  |
| g            | Gravity (m/s)                           | eff           | Efficiency   |
| G            | Mass flux ( $kg/s$ )                    | fin           | Fin  |
| h            | Heat transfer coefficient ( $W.m^2C$ )  | hs            | Heat sink  |
| H            | Height (m)                              | i             | Vector unit i  |
| k            | Thermal conductivity ( $Wm.^{\circ}C$ ) | j             | Vector unit j  |
| K            | Turbulent kinetic energy ( $J/kg$ )     | s             | Surface  |
| L            | Length (m)                              | t             | Time   |
| n            | Number of fins                          | th            | Thermal  |
| Pr           | Prandtl number                          | $\infty$      | Ambient  |
| P            | Distance of fins                        | In            | In   |
| Q            | Power (W)D                              | Our           | Out  |
| q            | Heat flux ( $W/m^3$ )                   | th            | Thermal  |
| R            | Resistance                              |               |  |
| S            | Source term ( $W/m^3$ )                 | $\mu$         | <b>Greek symbol</b><br>Dynamic viscosity( $Ns/m^2$ ) |
| T            | Temperature ( $^{\circ}C$ )             | $\theta$      | Angle ( $^{\circ}$ )                                 |
| U            | Flow rate (m/s)                         | $\varepsilon$ | Transport  |
| V            | Kinematic viscosity ( $m^2.s$ )         | $\alpha$      | Molecular weight (kg/mol)                            |
| V            | Volume ( $m^3$ )                        |               |  |
| U            | Flow rate (m/s)                         | $\rho$        | Density ( $Ns/m^2$ )                                 |
| v            | Kinematic viscosity ( $m^2.s$ )         | $\eta$        | Ratio turbulent kinetic energy                       |
| W            | Fin thickness (mm)                      |               |  |
| x,y,z        | Axis direction                          |               |  |

Variations in geometric configurations such as horizontal fin arrangement, Circular arrangement [26,27]. The parallel arrangement of heat sink fins was characterized in experiments carried out by numerical methods to increase heat transfer and thermal resistance and reduce stress on the heat sink lines due to a dense and diverse thermal boundary layer [28]. Heat sink fins with double layer arrangement were investigated experimentally and numerically[29]. In addition, the geometric configuration of thickness, height, width or distance, and the number of fins can reduce heat and increase heat transfer in the heat sink to produce an excellent cooling system on heat sink because, in shorter channels, the flow tends to develop thermally and hydro dynamically [30-32].

The effect of flow rate can increase the thermal conductivity and good heat transfer coefficient on the heat sink, which is indicated by the increase in the efficiency value of 29.65% [33]. The incoming heat flux affects the heat transfer coefficient and heat sink performance. This can be proven by increasing the Nusselt number and fluid flow

Previous research focused on thermally and hydro dynamically developed flow to several variations such as fin height, number of fins, fin spacing, fin shape, mass flow rate, pressure, heating power, and so on. There is no numerical study on the effect of fin longitudinal spacingalongwiththeangle of oblique fin heat sinks on fluid flow and heat transfer oftheheat sinks.This study utilizes a finite-volume computational approach to determine the performance and details of the flow on the heat sinks. The calculations are conducted on fin spacing between 0.3 mm and 1.5 mm in the Reynolds number of 6,470 to 19,410.

## II. COMPUTATIONAL METHODS

### 2.1 Computational Domain

The heat sink geometry is made using Solid works drawing software which refers to the literature [41]. In this study, the heat sink design consists of several geometric arrangements, such as the fins' number, distance, and thickness. All sizes are considered constant except for the distance between the fins in the horizontal direction. The literature describes the effect of geometry on SFHS with various fin arrangements, which were studied with experimental and numerical approaches using the free convection method. Then we propose a novelty in this study, namely the variation in geometry in the form of shape, oblique angle, and the distance between the horizontal and vertical fins on the heat sink along with its size. Experimental and numerical studies from the literature [41] on the effect of geometric shape and arrangement of fins were investigated to find the most optimal heat sink design for heat transfer by the free convection method. In this study, the SFHS (Straight-FinnedHeatSinks) wasmodifiedtobecome OFHS (Oblique-FInHeatSink) with an oblique angle of  $45^{\circ}$  and variations in the distance between the fins in the horizontal direction of 0.3-1.5 mm. Figure 1 (a) and (b)showa geometric image of the top

and front views on OFHS with variations in the oblique angle of  $45^\circ$ , along with the size and data collection on the arrow lines ( $T_b$ ), ( $T_{ba}$ ) and ( $T_{s ave}$ ).

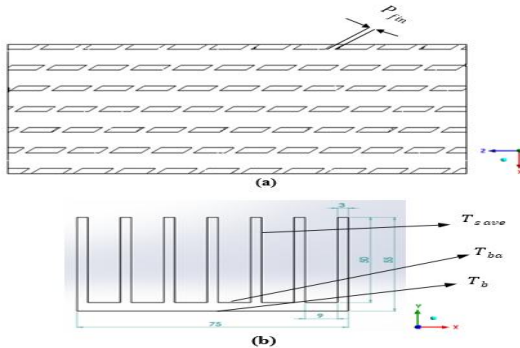


Figure 1: (a) Upper View and (b) Front View of the OFHS

### 2.2 Boundary Condition

We analyzed the heat transfer and flow fields using steady-state conjugate three-dimensional flow simulations. Radiation model on OFHS. The surface is considered for energy exchange between fin surfaces, based on their size, distance, and orientation, quantified by the geometric parameter display factor. Furthermore, absorption, emission, or scattering is assumed to be negligible. Therefore, the radiant energy flux from the fin surface consists of the emitted and reflected energy.

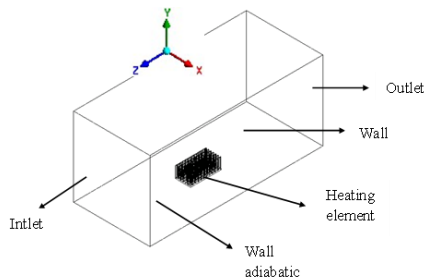


Figure 2: Computational Domain

The computational net used in the simulation is shown in Figure 3. A volume-based control technique is used to discretize the equation governing the first-order upwind scheme for higher accuracy.

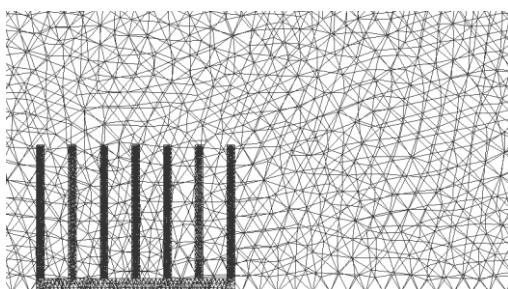


Figure 3: Tetrahedral Grid Structure

The boundary conditions used in this study are summarized as assumptions and limitations, which include:

1. The bottom surface of the heat sink is subjected to a constant heat flux.
2. In adiabatic conditions, i.e.  $\frac{\partial T}{\partial n} = 0$  is applied to the air wall at the bottom.
3. All walls are a non-slip boundary condition.
4. The boundary conditions at the front and rear air surfaces are defined as the inlet and outlet, while for the others, it is the wall.
5. The viscous model used is *k-ε Realizable* with a tetrahedral mesh structure.
6. The convergence conditions are all determined  $10^{-4}$  for flow and  $10^{-7}$  for energy, and the parameters to be achieved are the base ( $T_b$ ), temperature (OFHS surface temperature ( $T_{ave}$ ), fin surface temperature ( $T_{s ave}$ ) from OFHS to find the value of heat transfer coefficient and thermal resistance ( $R_{th}$ ).

The computational domain is discretized with a non-structured and high-resolution tetrahedral grid to capture the thermal boundary layer effect accurately. The compute domain is defined as 700 mm x 330 mm x 300 mm. Determination of the wall at the boundary conditions, which can be seen in Figure 2, namely the numerical analysis of single-phase flow through oblique fins in a steady state. Reynolds mean and Navier-Stokes continuity equations are solved using the *k-ε Realizable* turbulence model, which can solve numerical equations quickly, precisely, and accurately and depends on the assumptions in the selected viscous model [42].

### 2.3 Turbulence Model

The governing equations in the three-dimensional computational domain for heat sinks are the conduction equations written in Cartesian coordinates, the Reynolds continuity means, and the Navier-Stokes equations can be written in tensor notation as:

$$\frac{\partial}{\partial x_i}(\rho u_i) = 0 \tag{1}$$

$$\frac{\partial}{\partial x_j}(\rho u_i u_j) \frac{\partial p}{\partial x_i} + \frac{\partial}{\partial x_j} \left[ \mu \left( \frac{\partial u_i}{\partial x_j} + \frac{\partial u_j}{\partial x_i} \right) - \overline{\rho u_j u_j} \right] \tag{2}$$

Where  $\overline{\rho u_j u_j}$  calculates turbulent stress:

$$-\overline{\rho u_j u_j} = \mu_t \left( \frac{\partial u_i}{\partial x_j} + \frac{\partial u_j}{\partial x_i} \right) \tag{3}$$

To obtain the kinetic energy and the rate of dissipation of kinetic energy for turbulence, it is necessary to use the *k-ε*

Realizable equation obtained from the modification of the k-ε Standard equation so that it becomes:

$$\frac{\partial}{\partial x_i}(\rho k u_i) \frac{\partial}{\partial x_j} \left( \alpha_k \mu_{eff} \frac{\partial k}{\partial x_j} \right) + G_k - \rho \epsilon + S_k \quad (4)$$

$$\frac{\partial}{\partial x_i}(\rho \epsilon u_i) \frac{\partial}{\partial x_j} \left( \alpha_\epsilon \mu_{eff} \frac{\partial \epsilon}{\partial x_j} \right) + C_{1\epsilon} \frac{\epsilon}{k} C_{2\epsilon}^* \rho \frac{\epsilon^2}{k} \quad (5)$$

Where  $S_k$  is defined as the source of user-defined terms on turbulence kinetic energy, and  $G_k$  is the generation of turbulent kinetic energy due to the average velocity gradient calculated by equation (6):

$$G_k = \mu_t \left( \frac{\partial u_i}{\partial x_j} + \frac{\partial u_j}{\partial x_i} \right) \frac{\partial u_i}{\partial x_j} \quad (6)$$

Turbulence and effective viscosity are defined as  $\mu_t$  and  $\mu_{eff}$  with the following equations:

$$\mu_t = \rho C_\mu \frac{k^2}{\epsilon} \quad (7)$$

$$\mu_{eff} = \mu + \mu_t \quad (8)$$

$C_{2\epsilon}^*$  is a constant modification is  $C_{2\epsilon}$  written:

$$C_{2\epsilon}^* = C_{2\epsilon} \frac{C_\mu \eta^3 (1-\eta) / \eta_0}{1 + \beta \eta^3} \quad (9)$$

Where is the ratio of user-defined turbulence kinetic energy to turbulence kinetic energy dissipation rate, where  $\eta = S_k / \epsilon$ . When the value  $\eta$  is not too high or when weak or moderate strain flow, the value  $C_{2\epsilon}^*$  and  $C_{2\epsilon}$  is close to each other. Therefore, the viscous model k-ε Realizable gives great results approaches to the standard k-ε turbulence model. When the value of  $\eta$  higher than  $\eta_0$ , then the flow is very strong so that the value of  $C_{2\epsilon}^*$  smaller than  $C_{2\epsilon}$  would have predicted the turbulence model to standard. Equation (5) results in lower crushing than usual. As the destruction decreases, the value increases, resulting in a lower k. An increase in and a decrease in k results  $\mu_t$  in a lower [43].

## 2.4 Grid Independence

The sizes and models of OFHS, along with the computational domains, are shown in Figures 1 and 2. Grid Independence is carried out to determine the optimum point of the experimental value in the form of the base temperature of the heat sink ( $T_b$ ), the average surface temperature of the heat sink ( $T_{ba}$ ) calculated on the surface of the bottom ( $T_{s\ ave}$ ) heat sink, while the surface temperature of the fins is calculated on all surfaces of the heat sink fins. The grid test is carried out by considering the size of the number of mesh cells in the

computational domain between 634360, 774320, 817800, and 931900.

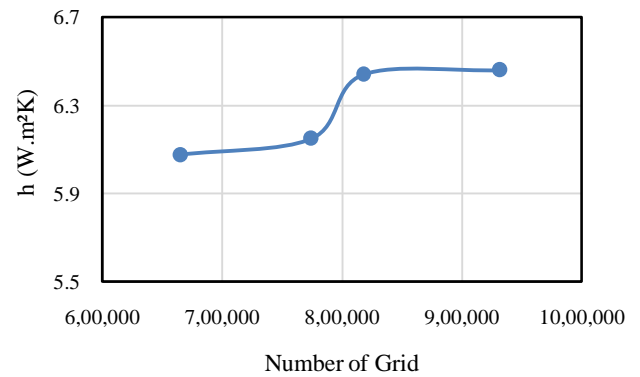


Figure 4: Effect of Grid Numbers of Heat Transfer in Heat sinks

Grid test results are presented as a graph of the relationship between the grid number and the value of the heat transfer coefficient. Calculations on numerical studies in the grid test shown in Figure 4 relative error between grids 634360 with 774320 is  $\pm 3\%$ , 774320 with 817800 is  $\pm 2\%$ , and 817800 with 931900 is  $\pm 0.1\%$ .

## 2.5 Computational Setup

OFHS analyzed the heat transfer and flow field under steady conditions in a three-dimensional flow simulation. Numerical simulations are required to gain insight into flow migration through OFHS to evaluate the thermal and hydraulic performance obtained from flow paths. For this purpose, steady-state fluid flow and heat transfer are simulated. The k-ε Realizable turbulence model was chosen because of its fast, precise, and accurate completion compared to other k-ε models by considering the results of the literature validation. With an improved computational domain and use on incompressible airflow. Thermal and air transport properties are taken as functions of temperature. Viscous dissipation, radiant heat transfer, and ignoring body forces.

The details of the computational domain modelling are shown in Figure 2, which was made with experimental considerations from [41]. The figure is a picture of the overall geometry of the heat sink. In the figure, the airflow in the three-dimensional computational domain with free and forced convection methods is carried out with steady air conditions and assumed with constant thermal physical properties. In addition, convection heat transfer between a heatsink and air interface is considered in OFHS.

The convergence criteria for flow are  $10^{-4}$  and  $10^{-7}$  for energy. The nature of the free air that acts as a coolant in this numerical study is air with material properties density = 1.2096 kg/m<sup>3</sup>, specific heat capacity  $C_p = 1005$  J/kg.K, viscosity =  $1.915 \times 10^{-5}$  kg/ms, thermal conductivity  $k = 0.0261$

W/m. K, and molecular weight 28,966 kg/kmol. For all simulations, the inlet temperature is set at 25°C. Aluminium alloy 6061 is used for the heatsink module, and thermal conductivity is assumed to be  $k = 168$  (W/mK) with  $Q = 50$  W. Non-slip walls are specified for finsurfaces at boundary conditions.

### 2.6 Numerical Data Reduction

The average air velocity in the OFHS channel is between 1-19 m/s, and the number of oblique fins consists of 7 rows. The average for the Reynolds number is:

$$Re = \frac{\rho \cdot D_h \cdot U_\infty}{\mu} \quad (10)$$

Where the equation defines the hydraulic diameter:

$$D_h = \frac{4s \cdot H}{2(H \cdot s)} \quad (11)$$

The equation can calculate OFHS surface area:

$$(nLH) + (PL) \quad (12)$$

The equation can calculate the OFHS base area:

$$2(LP) \quad (13)$$

The pressure drop through OFHS is calculated by taking the difference between the static pressure on the air inlet and outlet sides, so the pressure drop equation is:

$$\Delta P = P_{in} - P_{out} \quad (14)$$

Thermal resistance and heat transfer coefficient can be calculated using the following equation:

$$R_{th} = \frac{T_{ave} - T_\infty}{Q} \quad (15)$$

$$h = \frac{Q}{A_b (T_{s\ ave} - T_\infty)} \quad (16)$$

Convective heat transfer coefficient  $h$ (W/m<sup>2</sup>.K) and the pressure drop are expressed in Colburn factor  $j$ , and friction factor  $f$  is a dimensionless factor so that:

$$j = \frac{Nu}{Re Pr^{1/3}} \quad (17)$$

$$f = \frac{\Delta P D_h}{2 \rho u_{in}^2 L} \quad (18)$$

The Nusselt number in the equation:

$$Nu = \frac{h \cdot D_h}{k} \quad (19)$$

### III. RESULTS AND DISCUSSION

In this study, we present several results related to simulation testing on OFHS specimens with various variations, such as oblique angles and horizontal and vertical gravity directions, using the free convection method for validation. Then we also propose numerical simulations on OFHS for variations in oblique angle, the distance between fin gaps in the horizontal direction, and various Reynolds numbers to optimize the OFHS design on the heat transfer rate.

#### 3.1 Validation

The calculation is carried out if all the boundary condition data have been determined. The number of iteration processes affects the level of accuracy obtained. The model's accuracy level influences the determination of the number of iterations. The more grids used in the modelling, the more iterations need to be done to calculate the model. The iteration process stops when it reaches the predetermined convergence limit. The calculation is carried out to the smallest error value, or a convergent value is obtained [45].

Validation is carried out through a numerical approach to experiments conducted by the literature [41] on heat sink specimens with the free convection method. The parameters to be sought in this study are parameters  $T_b, T_{ba}, T_{s\ ave}$ . Validation is conducted with variations such as the number of grids, viscous models, and methods.

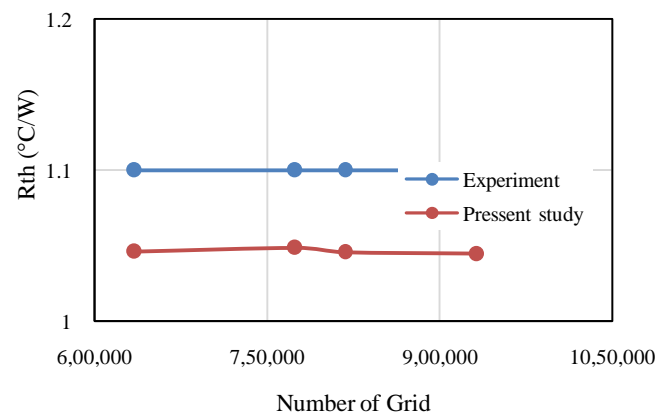


Figure 5: Relationship between Grid Number and Thermal Resistance

The results of the validation are presented in Figure 5. The relationship between the grid number and the thermal resistance of the heat sink on the graph can be seen from the experimental results carried out by the literature [41] on the SFHS-type heat sink. The value of the thermal resistance of the heat sink is 1.1° C/W. The results of free convection simulations to experiments from the literature in thermal resistance have the largest relative error of 5.2%, with a value

of 1.04 (°C/W) for various viscous models of k-ε and method. For various viscous models, k-ω and method have the largest relative error with a value of 5.4% with a thermal resistance value of 1.02 (°C/W). These results indicate a good agreement between the experimental results in the literature and the numerical study being validated.

The results of SFHS validation against experimental literature [41] on SFHS, which are being validated with various variations of viscous models and methods, significantly affect the heat transfer rate. It is characterized by a decrease in temperature at the fin surface, allowing for optimal SFHS-related design and manufacture. In addition, the consideration of maintenance of SFHS becomes easier.

### 3.2 OFHS Heat Transfer Characteristics

OFHS optimization with variations in oblique fin geometry with an oblique angle of 45°, variations in the distance between fins in the horizontal direction of 0.3-1.5 mm, and variations in air flow rates between 5-15 kg/s were investigated to find the most optimal design for OFHS. The heat transfer coefficient is strongly related to the incoming heat flux for the heat sink specimen. In the experiment conducted by the literature [41], the heat transfer coefficient value was calculated based on the average temperature value on the fins of all OFHS surfaces.

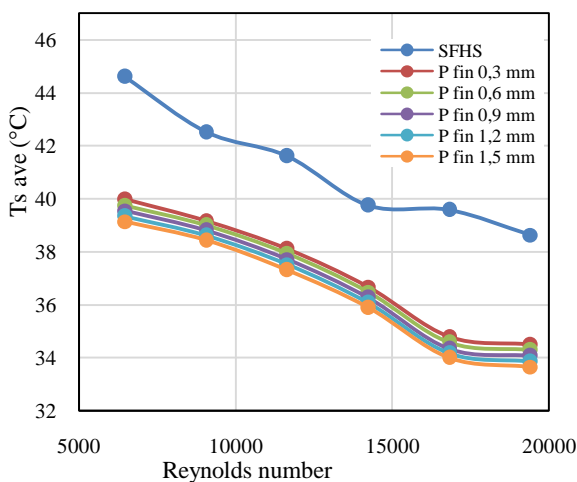


Figure 6: The Relationship between Reynolds Number and Average Temperature of Fin Surface

The OFHS surface temperature value is taken when the heat sink is in a steady state, so the temperature distribution in the fin surface area is very even. In addition, the oblique angle and the distance between the fins also have a strong enough force on the heat transfer coefficient. This is due to the thin initialization of the thermal boundary layer between the oblique angle and the fin gap, even under the same operating conditions and mechanism.

Figure 6 is a graph of the relationship between the Reynolds number and the simulation results in the form of temperature parameters on the surface of fins. Temperature fluctuations that occur in OFHS with variations in the distance between the fins are 0.3 mm is caused by insufficient intake air pressure. The air tends to shift rapidly towards the trajectory of the large slit, affecting the fins' surface temperature. The average surface temperature of the fins on the OFHS ranged between 34.49°C and 34.29°C.

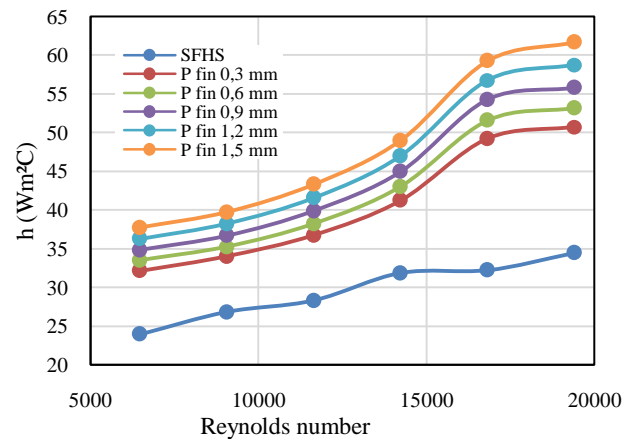


Figure 7: Relationship between Reynolds Number and Heat Transfer Coefficient Parameters in OFHS

The difference in the average surface temperature of OFHS allows the heat transfer coefficient to be more effective. Figure 7 depicts the influence of heat transfer coefficient on fin longitudinal for various Reynolds numbers at an oblique angle of 45°. The Reynolds number plays an essential role in the heat transfer coefficient. In the figure, it is explained that the greater the Reynolds value, the greater the value of the heat transfer coefficient. Increasing the Reynolds number makes it possible to cool the fin surface on both SFHS and OFHS. The comparison of heat transfer coefficient values between SFHS and OFHS is very significant, ranging from 10 Wm<sup>2</sup>.C to 12Wm<sup>2</sup>.C so that the performance of SFHS and OFHS can be improved and can help optimize the performance of electronic components.

In Figures 6 and 7, the temperature of OFHS, the average surface temperature of the fins, and the heat transfer coefficient on OFHS tend to differ significantly from that of SFHS. OFHS geometry tends to provide many gaps or space for fresh air in the oblique bends, resulting in optimal cooling. In contrast, for SFHS geometry, the airflow tends to follow the direction of the fins, so the cooling process is less than optimal. Figure 8-10 shows the OFHS temperature contour with a distance between the fins of 1.5 mm in various axis directions.

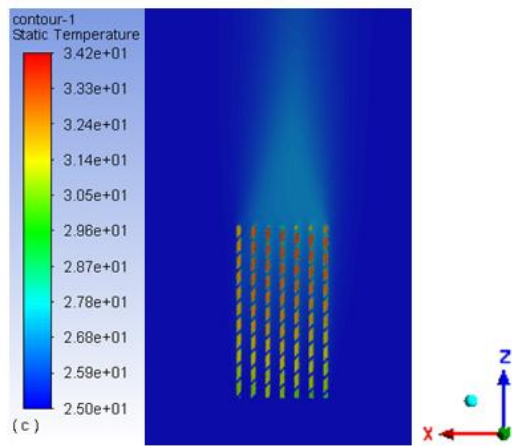


Figure 8: Temperature Contours of OFHS with 1.5 mm fin spacing at x - z plane (Height y = 5 mm)

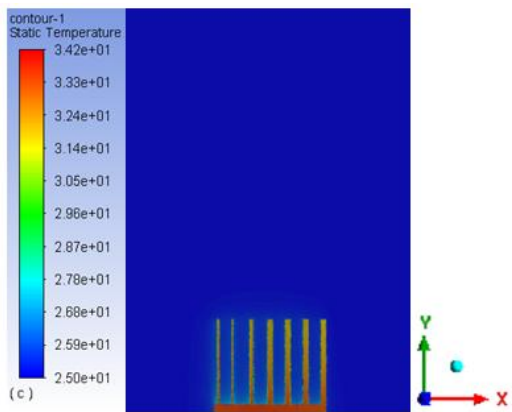


Figure 9: Temperature Contours of OFHS With a Distance Between Fins of 1.5 mm at x - y plane Direction (z = 4 50 mm)

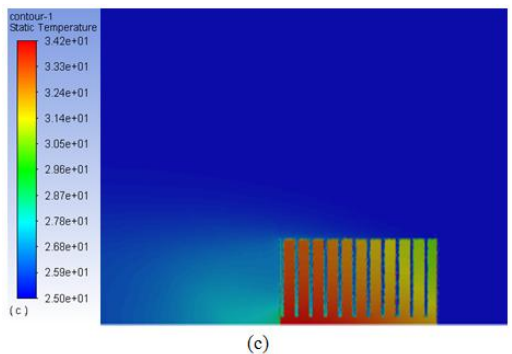


Figure 10: Contour of Temperature of OFHS with 1.5 mm fin spacing at y - z plane (x = 150 mm)

Induced flow migration via an oblique finned micro channel cooler operating in conventional flow has proven to affect the uniformity of the surface temperature of the fins. This is due to temperature fluctuations after reaching a steady state. The flow migrates at an oblique angle of  $45^\circ$  with a variation of the distance between the fins of 1.5 mm so that the temperature uniformity on the OFHS surface increases. Oddly, OFHS with an oblique angle of  $45^\circ$  with a variation of the

distance between the fins of 0.3 mm experienced a more severe flow migration and had a less consistent cumulative secondary flow distribution. This is because the flow tends to pass through the gap between the fins due to the narrow field but can maintain a more uniform wall temperature distribution, as shown in Figures 11-13. With these factors, the angle and distance between the oblique fins on OFHS significantly affect heat transfer in OFHS so that OFHS can work effectively for the cooling process of microelectronic components.

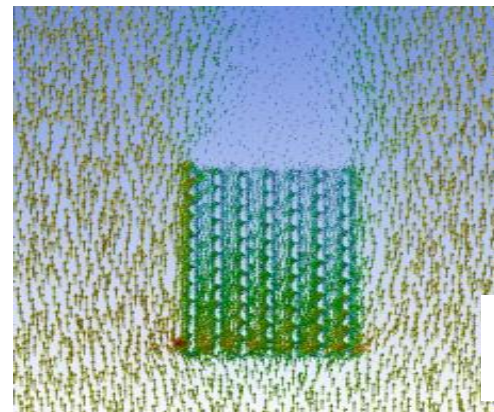


Figure 11: Vector Velocity on OFHS with a Distance between Fins of 1.5 mm at x - z plane (Height y = 5 mm)

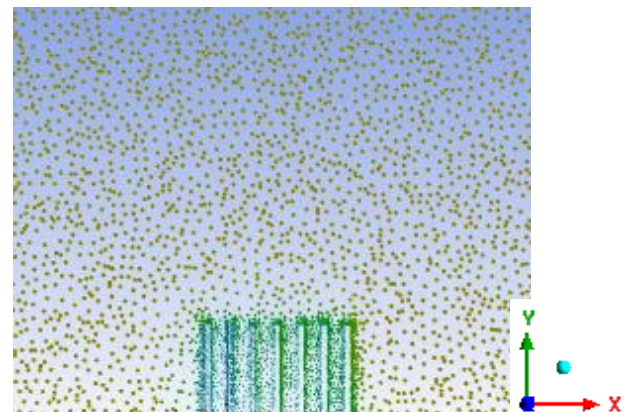


Figure 12: Velocity Vector on OFHS with 1.5 mm fin spacing at x - y plane (z = 4 50 mm)

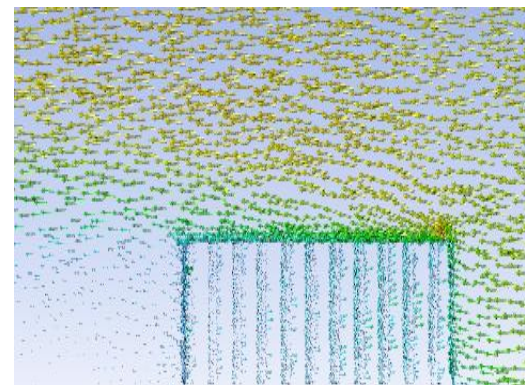


Figure 13: Velocity Vector on OFHS with 1.5 mm Fin Spacing at y - z Plane (x = 150 mm)

### 3.3 Effect of Longitudinal Fin Spacing on Base Temperature

OFHS, which we propose and investigate for their heat transfer, some OFHS configurations with oblique angles between 45° were studied. The configuration of constant fin spacing for the free convection method and variations in the oblique fin spacing ranged from 0.3-1.5 mm in various Reynolds numbers for forced convection.

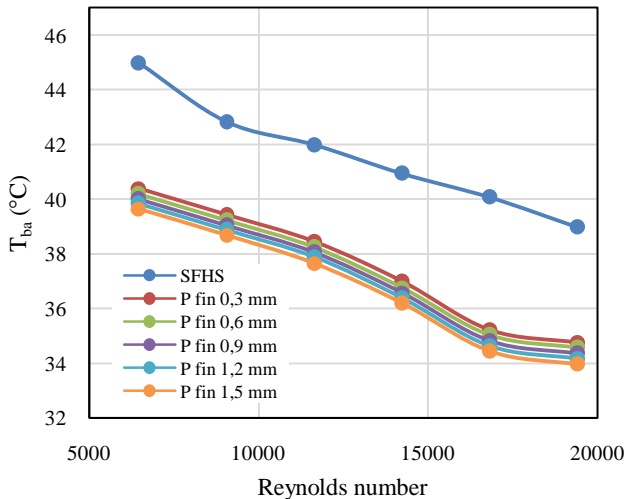


Figure 14: Relationship between Reynolds Number and Base Temperature

The continuous induced flow pattern of the secondary flow then migrates, resulting in improper flow distribution. The results can be seen in Figure 14 as the relationship between the Reynolds number and the simulation results in the form of the base temperature parameter. A larger oblique angle allows fresh air to enter freely without obstacles into the gap. The angle also provides a higher velocity so the free air can initialize the flow repeatedly. Thus this result verifies the validity of the optimal design algorithm in estimating the optimized O form of FHS under conditions of forced convection operation.

Changes in temperature in flow due to oblique angle are small enough to allow simulation of constant properties on OFHS and imply that buoyancy is negligible. A significant increase in Reynolds number resulted in disturbance of the boundary layer in the gap between the fins. It is proven that the base temperature in OFHS slowly decreases as the Reynolds number increases. The base temperature tends to drop sharply at the Reynolds number between 6470-16822. It is proven that the base temperature difference is at Reynolds number 6470 at OFHS with a distance between fins of 0.9 mm at 40°C and 34.81°C when Reynolds number is 16822.

The simulation results of the heat sink with oblique fins show that the developed air flow provides a favourable

secondary flow distribution. Preliminary quantitative interpretation of simulation results can improve heat transfer and reduce the pressure drop penalty from OFHS. Various intake air flow rates provide good thermal and hydraulic performance data. In contrast, base temperature measurements provide insight into the uniform surface temperature of the underside of the fin to determine the thermal resistance of the OFHS.

### 3.4 Effect of Longitudinal Fin Spacing on Thermal Resistance

Figure 15 implies a significant increase at a high Reynolds number resulting in a sharp decrease in thermal resistance value. In boundary layer disturbance in the gap between the fins, the air entering the OFHS gap tends to be irregular because of the bend in the form of an oblique angle. Air continuously initializes the gap between the fins to create a new boundary layer resulting in a uniform temperature difference between the fins.

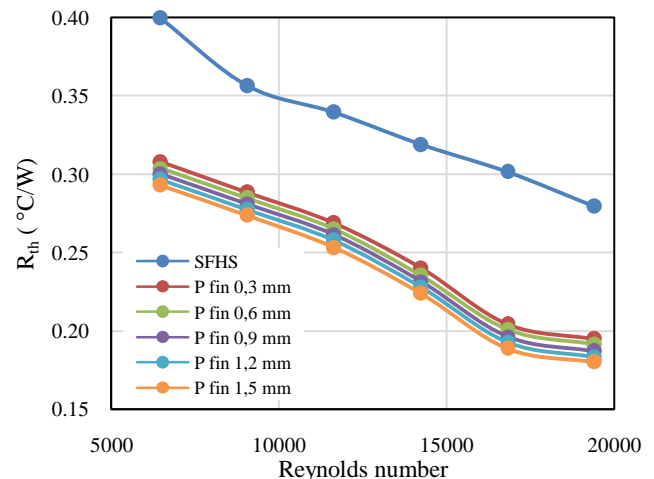


Figure 15: Effect of Reynolds Number on Thermal Resistance

Nevertheless, the air that enters the OFHS gap is uniquely irregular because the deflection is at an oblique angle. At higher Reynolds numbers, the flow is transitional or turbulent. The air continues to initialize the gap between the fins to create a new boundary layer, resulting in a uniform temperature difference between the fins. Therefore, the heat sink micro channels with variations in the angle of inclination can be conclusively concluded to the reference value of the thermal resistance.

### 3.5 Effect of Longitudinal Fin Spacing on Bottom Temperature

Several studies on the variation of the distance between the fins on the heat transfer rate were carried out by several researchers [32,34]. However, this study considered the effect

of the distance between the oblique fins. Numerical simulation on OFHS with forced convection method at an oblique angle of 45° with a distance between the oblique fins between 0.3-1.5 mm indicates a difference in the heat transfer rate, but the difference is enormous. Figure 16 shows the Reynolds number and bottom temperature relationship at various distances with an oblique angle of 45°. The relative temperature decreased in various variations of the distance between the fins for all variations of fin distances. There is a possibility that flow and heat transfer in ducts are not fully developed when the fin spacing is small and allows a thicker boundary layer resulting in poor heat transfer.

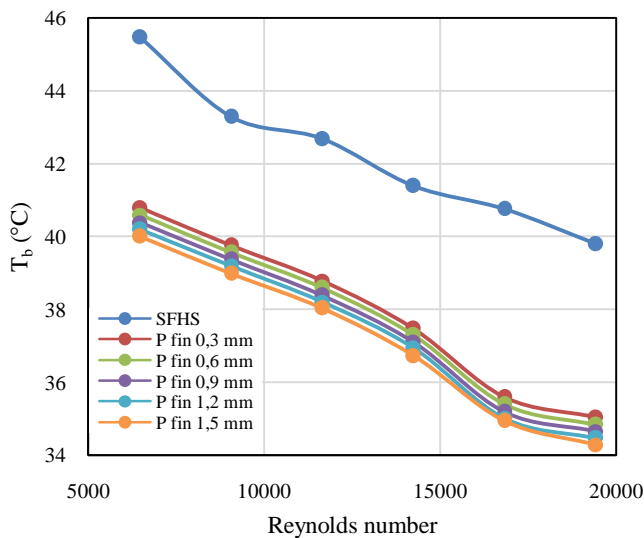


Figure 16: Effect of Reynolds Number on Bottom Temperature

It is proven in the simulation results of the bottom temperature on the bottom surface of OFHS with a distance between the fins of 0.3 mm, indicating the magnitude of the temperature value. The temperature value is 40.78°C at the Reynolds number 6470, with the same Reynolds number but at a different distance between syrups, 1.5 mm.

The bottom temperature value on OFHS is 40°C. The difference in temperature due to the distance between the fins represents that of OFHS. The large fin spacing allows good heat transfer so that the OFHS performance can be considered for cooling applications in microelectronic components.

For large fin spacing, the average temperature and heat transfer coefficient grow with decreasing surface temperature under significant OFHS. Since the air inlet of the oblique fin mainly along the direction oblique to decrease in fin spacing, the thermal limit thinning layer at the inlet contributes to a high local heat transfer coefficient, especially when the bonded thermal layer moves from full expansion to incomplete expansion.

### 3.6 Effect of Longitudinal Fin Spacing on Nusselt Number

In Figure 17, the distance between the fins increases the Nusselt number, and the convection heat transfer increases due to variations in the distance between the fins, allowing the airflow in OFHS to move freely towards the fin gap. Unlike the case with SFHS, where the airflow tends to be constant straight following a square cross-section to allow poor heat transfer. Comparing the Nusselt number values in SFHS and OFHS is very significant. At Reynolds 19410, the Nusselt number for SFHS is 33.53. While at the same Reynolds number on OFHS with a distance between fins of 1.5 mm is 42.10. This is due to the various temperature differences on each surface of the heat sink fin. The temperature difference at the heat sink surface is caused by the induction of flow around the fin surface and continuously initializes the thermal and hydraulic boundary layers.

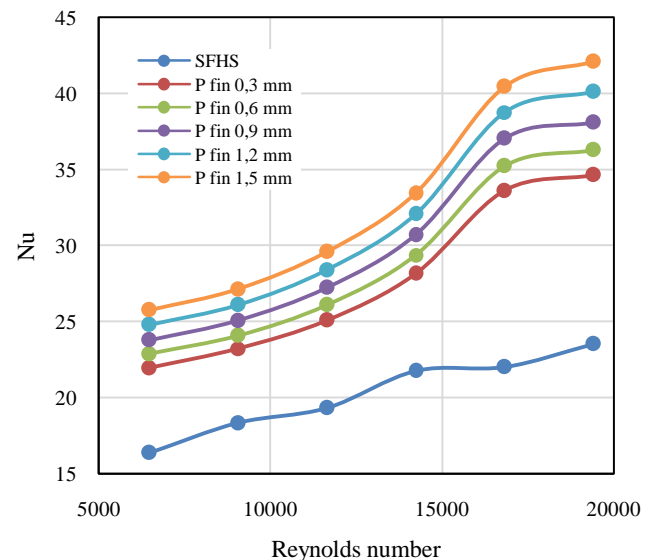


Figure 17: Relationship between Reynolds Number and Nusselt number

## IV. CONCLUSION

It was found that the fin longitudinal spacing significantly affects the performance of heat sinks for various Reynolds numbers, where the larger the spacing, the higher the Nusselt number. Based on this study, it can be concluded that it is necessary to determine the optimal fin longitudinal spacing in the design of the oblique heat sink.

## ACKNOWLEDGEMENT

This work was supported by the Indonesian Education Scholarship (Beasiswa Pendidikan Indonesia) 2020 – 2022 under the Indonesian Ministry of Education, Research, Culture, and Technology. Jl. General Sudirman, Senayan, Jakarta (10270) Indonesia.

## CONFLICT OF INTEREST

The authors state that we are unaware of any competing financial interests or personal relationships that may appear to influence the work reported in this paper.

## REFERENCES

- [1] F. Han, H. Guo, and X. Ding. "Design and optimization of a liquid-cooled heat sink for a motor inverter in electric vehicles." *Apps. Energy*, vol. 291, pp. 1-14, January 2021. doi: 10.1016/j.apenergy.2021.116819.
- [2] AMA Mageeth, SJ Park, M. Jeong, W. Kim, and C. Yu. "Planar-type thermally chargeable supercapacitor without an effective heat sink and performance variations with layer thickness and operation conditions," *Appl. Energy*, vol. 268, pp. 1-9, October 2019. doi: 10.1016/j.apenergy.2020.114975.
- [3] D. Kong, Y. Kim, M. Kang, E. Song, Y. Hong, HS Kim, KJ Rah, HG Choi, D. Agonafer, H. Lee. "A holistic approach to the thermal-hydraulic design of 3D manifold microchannel heat sinks for energy-efficient cooling," *Case Stud. therm. eng.*, vol. 28, pp. 1-13, September 2021. doi:10.1016/j.csite.2021.101583.
- [4] M. Ghaneifar, H. Arasteh, R. M. ashayekhi, A. Rahbari, RB Mahani, and P. Talebizadehsardari. "Thermohydraulic analysis of hybrid nanofluid in a multilayered copper foam heat sink employing local thermal non-equilibrium condition: Optimization of layers thickness," *Appl. therm. eng.*, vol. 181, pp. 1-13, June 2020. doi: 10.1016/j.applthermaleng.2020.115961.
- [5] MR Attar, M. Mohammadi, A. Taheri, S. Hosseinpour, MP Fard, MH Sabzevar, A. Davoodi. "Heat transfer enhancement of conventional aluminium heat sinks with an innovative, cost-effective, and simple chemical roughening method," *Therm. science. eng. prog.*, vol. 20, pp. 1-10, September 2020. doi:10.1016/j.tsep.2020.100742.
- [6] A. Moradikazerouni, M. Afrand, J. Alsarraf, S. Wongwises, A. Asadi, and TK Nguyen. "Investigation of a computer CPU heat sink under laminar forced convection using a structural stability method," *Int. J. Heat Mass Transfer.*, vol. 134, pp. 1218-1226, December 2019. doi: 10.1016/j.ijheatmasstransfer.2019.02.029.
- [7] M. Pan, Z. Chen, and C. Li. "Experiment and simulation analysis of oriented cut copper fibre heat sink for LED water cooling," *Case Stud. therm. eng.*, vol. 24, pp. 1-17, February 2021. doi: 10.1016/j.csite.2021.100878.
- [8] H. Zu, W. Dai, Y. Li, K. Li, and J. Li "Analysis of enhanced heat transfer on a passive heat sink with high-emissivity coating," *Int. J. Therm. Science.*, vol. 166, pp. 1-10, March 2021. doi: 10.1016/j.ijthermalsci.2021.106971.
- [9] A. Abbas and CC Wang, "Augmentation of natural convection heat sink via displacement design," *Int. J. Heat Mass Transfer.*, vol. 154, pp. 1-14, April 2020. doi: 10.1016/j.ijheatmasstransfer.2020.119757.
- [10] H. Hassan and NYA Shafey. "3D study of convection-radiation heat transfer of electronic chip inside enclosure cooled by a heat sink," *Int. J. Therm. Science.*, vol. 159, pp. 1-15, September 2021. doi:10.1016/j.ijthermalsci.2020.106585.
- [11] Y. Yoon, DR Kim, and KS Lee, "Cooling performance and space efficiency improvement based on heat sink arrangement for power conversion electronics," *Appl. therm. eng.*, vol. 164, pp. 1-10. September 2019. doi:10.1016/j.applthermaleng.2019.114458.
- [12] TW Ting, YM Hung, and N. Guo, "Effects of streamwise conduction on the thermal performance of nanofluid flow in a microchannel heat sink," *Energy Convers. Manag.*, vol. 78, pp. 14-23, November 2014. doi:10.1016/j.enconman.2013.10.061.
- [13] Y.alihosseini, MZ Targhi, and MM Heyhat, "Thermo-hydraulic performance of wavy microchannel heat sink with oblique grooved finned," *Appl. therm. eng.*, vol. 189, pp. 1-11, August 2020. doi: 10.1016/j.applthermaleng.2021.116719.
- [14] JG Song, JH Lee, and IS Park, "Enhancement of the cooling performance of naval combat management system using heat pipe," *Appl. therm. eng.*, vol. 188, pp. 1-12, February 2021. doi: 10.1016/j.applthermaleng.2021.116657.
- [15] D. Jung, H. Lee, D. Kong, E. Cho, KW Jung, CR Kharangate, M. Iyengar, C. Malone, M. Asheghi, KE Goodson, H. Lee, "Thermal design and management of micro-pin fin heat sinks for energy-efficient three-dimensional stacked integrated circuits," *Int. J. Heat Mass Transfer.*, vol. 175, pp. 1-17, May 2021. doi: 10.1016/j.ijheatmasstransfer.2021.121192.
- [16] A. Rajalingam and S. Chakraborty, "Effect of shape and arrangement of micro-structures in a microchannel heat sink on the thermo-hydraulic performance," *Appl. therm. eng.*, vol. 190, pp. 1-16, February 2021. doi: 10.1016/j.applthermaleng.2021.116755.
- [17] H. Sait, "Cooling a plate lithium-ion battery using a thermoelectric system and evaluating the geometrical impact on the performance of heatsink connected to the system," *J. Energy Storage*, vol. 52, pp. 1-14, 2022. doi:10.1016/j.est.2022.104692.
- [18] Z. Soleymani, M. Rahimi, M. Gorzin, and Y. Pahanli, "Performance analysis of hotspot using geometrical and operational parameters of a microchannel pin-fin hybrid heat sink," *Int. J. Heat Mass Transfer.*, vol. 159, pp. 1-18, June 2020. doi: 10.1016/j.ijheatmasstransfer.2020.119757.

- 10.1016/j.ijheatmasstransfer.2020.120141.
- [19] H. Nemati, M. Moradaghay, MA Moghimi, and JP Meyer, "Natural convection heat transfer over horizontal annular elliptical finned tubes," *Int. Comm. Heat Mass Transfer.*, vol. 118, pp. 1-10, September 2020. doi:10.1016/j.icheatmasstransfer.2020.104823.
- [20] K. Zhang, MJ Li, FL Wang, and YL He, "Experimental and numerical investigation of natural convection heat transfer of W-type fin arrays," *Int. J. Heat Mass Transfer.*, vol. 152, pp. 1-13, January 2020. doi:10.1016/j.ijheatmasstransfer.2020.119315.
- [21] S. Meganathan, R. Arunkumar, and A. Ponshanmugakumar, "Numerical analysis of passive heat sink for different shapes," *Mater. Today Proc.*, vol. 46, no. 1, pp. 3749–3755, 2020. doi:10.1016/j.matpr.2021.02.014.
- [22] B. Kanargi, JMS Tan, PS Lee, and C. Yap, "A tapered inlet/outlet flow manifold for planar, air-cooled oblique-finned heat sinks," *Appl. therm. eng.*, vol. 174, pp. 1-18, January 2020. doi:10.1016/j.applthermaleng.2020.115250.
- [23] El Ghandouri, A. El Maakoul, S. Saadeddine, and M. Meziane, "Design and numerical investigations of natural convection heat transfer of a new rippling fin shape," *Appl. therm. eng.*, vol. 178, pp. 1-14, June 2020. doi:10.1016/j.applthermaleng.2020.115670.
- [24] AL Teh, YW Phoo, WM Chin, EH Ooi, and JJ Foo, "Forced convective heat transfer enhancement of 90° bend plate-fin heat sink with grid generated turbulence," *Chem. eng. res. Dec.*, vol. 156, pp. 226–239, 2020. doi:10.1016/j.cherd.2019.12.004.
- [25] Q. Zhu, K. Chang, J. Chen, X. Zhang, H. Xia, H. Zhang, H. Wang, H. Li, Y. Jin, "Characteristics of heat transfer and fluid flow in microchannel heat sinks with rectangular grooves and different shaped ribs," *Alexandria Eng. J.*, vol. 59, no. 6, pp. 4593–4609, 2020. doi:10.1016/j.aej.2020.08.014.
- [26] A. Abbas, F. Qasrawi, and CC Wang, "Investigation of performance augmentation for natural convective heatsink with the help of chimney," *Appl. therm. eng.*, vol. 178, pp. 1-14, June 2020. doi:10.1016/j.applthermaleng.2020.115586.
- [27] P. Gil, "Experimental investigation on heat transfer enhancement of air-cooled heat sink using multiple synthetic jets," *Int. J. Therm. Science.*, vol. 166, pp. 1-10, February 2021. doi:10.1016/j.ijthermalsci.2021.106949.
- [28] J. Pandey, A. Husain, MZ Ansari, and N. Al-Azri, "Performance analysis of cold plate heat sink with parallel channel and pin-fin," *Mater. Today Proc.*, vol. 44, pp. 3144–3149, March 2021. doi:10.1016/j.matpr.2021.02.819.
- [29] N. Patel and HB Mehta, "Experimental investigations on a variable channel width double layered mini channel heat sink," *Int. J. Heat Mass Transfer.*, vol. 165, pp. 1-21, November 2021. doi:10.1016/j.ijheatmasstransfer.2020.120633.
- [30] Y. Ma, A. Shahsavari, and P. Talebizadehsardari, "Two-phase mixture simulation of the effect of fin arrangement on first and second law performance of a bifurcation microchannels heatsink operated with biologically prepared water-Ag nanofluid," *Int. Comm. Heat Mass Transfer.*, vol. 114, pp. 1-18, March 2020. doi:10.1016/j.icheatmasstransfer.2020.104554.
- [31] DK Kim, "Thermal optimization of plate-fin heat sinks with fins of variable thickness under natural convection," *Int. J. Heat Mass Transfer.*, vol. 55, no. 4, pp. 752–761, November 2012. doi:10.1016/j.ijheatmasstransfer.2011.10.034.
- [32] RC Adhikari, DH Wood, and M. Pahlevani, "An experimental and numerical study of forced convection heat transfer from rectangular fins at low Reynolds numbers," *Int. J. Heat Mass Transfer.*, vol. 163, pp. 1-12, August 2020. doi:10.1016/j.ijheatmasstransfer.2020.120418.
- [33] A. Torbatinezhad, AA Ranjbar, M. Rahimi, and M. Gorzin, "A new hybrid heatsink design for enhancement of PV cells performance," *Energy Reports*, vol. 8, pp. 6764–6778, May 2022. doi:10.1016/j.egy.2022.05.050.
- [34] AK Rao and V. Somkuwar, "Heat transfer of a tapered fin heat sink under natural convection," *Mater. Today Proc.*, vol. 46, pp. 7886–7891, March 2021. doi:10.1016/j.matpr.2021.02.565.
- [35] M/ Shoaib, SY Khan, N. Ahmed, M. Mahmood, A. Waqas, MA Qaisrani, N. Shehzad, "Thermal management of solar photovoltaic module by using drilled cylindrical rods integrated with phase change materials," *J. Energy Storage*, vol. 52, pp. 1-15, May 2022, doi:10.1016/j.est.2022.104956.
- [36] Z. Zhong, L. Meng, X. Li, G. Zhang, Y. Xu, and J. Deng, "Enhanced heat transfer performance of optimized micro-channel heat sink via forced convection in cooling metal foam attached on copper plate," *J. Energy Storage*, vol. 30, pp. 1-10, February 2020. doi:10.1016/j.est.2020.101501.
- [37] Y. Lin, Y. Luo, W. Li, Y. Cao, Z. Tao, and TIP Shih, "Single-phase and Two-phase Flow and Heat Transfer in Microchannel Heat Sink with Various Manifold Arrangements," *Int. J. Heat Mass Transfer.*, vol. 171, pp. 1-11, May 2021. doi:10.1016/j.ijheatmasstransfer.2021.121118.
- [38] S. Yan, F. Wang, J. Hong, and O. Sigmund, "Topology optimization of microchannel heat sinks using a two-layer model," *Int. J. Heat Mass Transfer.*, vol. 143, pp.

- 1-16, August 2019. doi: 10.1016/j.ijheatmasstransfer.2019.118462.
- [39] VS Bhandari and SH Kulkarni, "Optimization of heat sink for thyristor using particle swarm optimization," *Results Eng.*, vol. 4, pp. 1-4 June 2019. doi: 10.1016/j.rineng.2019.100034.
- [40] S. Rostami, AA Nadooshan, A. Raisi, and M. Bayareh, "Effect of using a heatsink with the nanofluid flow and phase change material on thermal management of plate lithium-ion battery," *J. Energy Storage*, vol. 52, pp. 1-31, August 2022. doi: 10.1016/j.est.2022.104686.
- [41] CH Huang and WY Chen, "A natural convection horizontal straight-fin heat sink design problem to enhance heat dissipation performance," *Int. J. Therm. Science.*, vol. 176, pp 1-13 January 2022. doi: 10.1016/j.ijthermalsci.2022.107540.
- [42] M. Law, OB Kanargi, and PS Lee, "Effects of varying oblique angles on flow boiling heat transfer and pressure characteristics in oblique-finned microchannels," *Int. J. Heat Mass Transfer.*, vol. 100, pp. 646–660, May 2016. doi: 10.1016/j.ijheatmasstransfer.2016.04.077.
- [43] CT Shaw *et al.*, "CT Shaw, Using Computational Fluid Dynamics, Prentice Hall. " *Techniques*, 1992.
- [44] TR Taha, " *An Introduction to Parallel Computational Fluid Dynamics*", vol. 6, no. 4. 2005. doi:10.109/mcc.1998.736434.
- [45] HJ Ferziger and M. Peric, "Computational Methods for Fluid Dynamics". third, rev. editions. vol. 7, no. 1. 2015. ISBN 3-540-42074-6, Springer-Verlag Berlin Heidelberg New York.

**Citation of this Article:**

Muhamad Safi'i, Nazaruddin Sinaga, Syaiful, Sukiman, "Computational Study of the Effect of Fin Longitudinal Spacing and Reynolds Number on the Performance of Oblique Heat Sinks" Published in *International Research Journal of Innovations in Engineering and Technology - IRJIET*, Volume 6, Issue 9, pp 27-38, September 2022. Article DOI <https://doi.org/10.47001/IRJIET/2022.609004>

\*\*\*\*\*